Near-field and SERS enhancement from rough plasmonic nanoparticles

Andreas Trügler,[1] Jean-Claude Tinguely,[1] Georg Jakopic,[2] Ulrich Hohenester,[1] Joachim R. Krenn,[1] and Andreas Hohenau[1]
[1]*Institut für Physik, Karl-Franzens-Universität Graz, Universitätsplatz 5, 8010 Graz, Austria*
[2]*Materials Institute for Surface Technologies and Photonics, Joanneum Research Forschungsgesellschaft mbH, 8160 Weiz, Austria*
(Received 2 December 2013; revised manuscript received 24 March 2014; published 8 April 2014)

The lithographic fabrication of metal nanoparticles usually involves the thermal vacuum deposition of metals, which leads to polycrystallinity and surface roughness. In recent years, strong efforts have been made to clarify the role of such roughness in surface-enhanced Raman scattering (SERS). In this paper, we provide a systematic experimental and theoretical study of single lithographically fabricated nanoparticles to unravel the role of surface roughness and morphology on the optical far- and near-field properties. We find that the experimentally observed reduction of the SERS signal upon thermal annealing of particle arrays is caused by a complex interplay of changes in the dielectric response of gold, the resonance wavelength, and the reduced nanoscopic roughness.

DOI: 10.1103/PhysRevB.89.165409 PACS number(s): 73.20.Mf, 78.30.−j, 03.50.De, 78.67.Bf

I. INTRODUCTION

Size inaccuracies and nanoscale surface roughness are inherent in practically all fabricated metallic nanoparticles [1,2] and lead to deviations of the optical properties from those of idealized nanoparticles [3,4]. Particularly, top-down approaches (like electron beam lithography) often involve vacuum deposition of the metal structures, which usually gives rise to polycrystalline particles with surface roughness and occasional remaining liftoff artifacts [2]. It has recently been shown [5] that a moderate amount of surface roughness has no significant impact on the far-field optical properties of metallic nanoparticles, but no corresponding conclusions hold for the near-field regime. In particular, for surface-enhanced Raman spectroscopy (SERS), surface quality is known to play a crucial role. Nanometric surface features can lead to large local variations in the optical field enhancements, as the local SERS enhancement is approximately proportional to the fourth power of the electric field enhancement [6].

Previously, we have shown [4] that after thermal annealing of gold nanoparticle arrays the measured SERS intensity decreases. This was attributed to annealing-induced changes in surface roughness, the average crystallite grain size of the polycrystalline gold nanoparticles [7], and the gold dielectric function [2,8]. However, the relative importance of these changes could not be addressed separately from the experiments alone. In this paper, we present a combined experimental and computational study to clarify the role of roughness and changes in the dielectric function for optical far- and near-field properties, as well as SERS enhancement of single gold nanoparticles. We start with a detailed experimental characterization of features typical for lithographically fabricated metal nanoparticles and their changes upon thermal annealing and then separately introduce these various material and morphology features in our simulation approach to investigate their respective importance. Most importantly, we find that the experimentally observed reduction of SERS signals upon thermal annealing of particle arrays is caused by a complex interplay of changes in the dielectric response of gold, the resonance wavelength, and the reduced nanoscopic roughness.

II. EXPERIMENTAL CHARACTERIZATION

In Ref. [4] we demonstrated that after a 200 °C thermal annealing process the measured SERS intensity on gold nanoparticle arrays decreases. Typical roughness features include roughness of the particle top surface and, for some particles, roughness (protrusions) at the particles' lateral boundaries [Fig. 1(a), arrows], most likely as a result of an imperfect liftoff process. Additionally, the particles sidewalls deviate slightly from a cylindrical shape, and rounding of the top and bottom edges can be observed.

Figure 1(b) shows scanning electron microscope (SEM) images of the same particles as in Fig. 1(a), but annealed for 5 min at 200 °C on a hot plate in air. At elevated temperatures, the mobility of surface and crystallite-interface atoms increases, thus causing surface-energy-driven morphology changes [7]. The comparison of the images before and after annealing shown in Fig. 1 reveals the virtual disappearance of edge roughness (protrusions) at the top edges [2,4], where atoms probably find energetically more favorable positions on the surface of the larger underlying crystallites. Further, larger surface areas bound by nearly straight, shallow grooves can be identified, which we interpret as crystallite boundaries, suggesting crystallite growth. Finally, the finer details at the particles' lateral boundary disappear upon annealing, and the images also hint at a slightly increased edge rounding, although no significant change in the particles' diameter was observed within the experimental uncertainty (±5 nm).

Apart from morphological changes, annealing also changes the gold dielectric function as depicted in Fig. 1(c). The data were obtained by spectroscopic ellipsometry on extended gold films prepared and annealed exactly like the gold nanoparticles before. To fit the ellipsometric data, the gold-film thickness was determined independently by atomic force microscopy (AFM), and the interfaces were assumed to be smooth.

Although the surface roughness of our films is on the order of only ∼1 nm rms value, which is very small compared to the wavelength range of visible light, it still could influence the ellipsometric measurements due to scattering of incident light and additional absorption through excitation of localized plasmon modes. To estimate the importance of these contributions, we included roughness in our model for

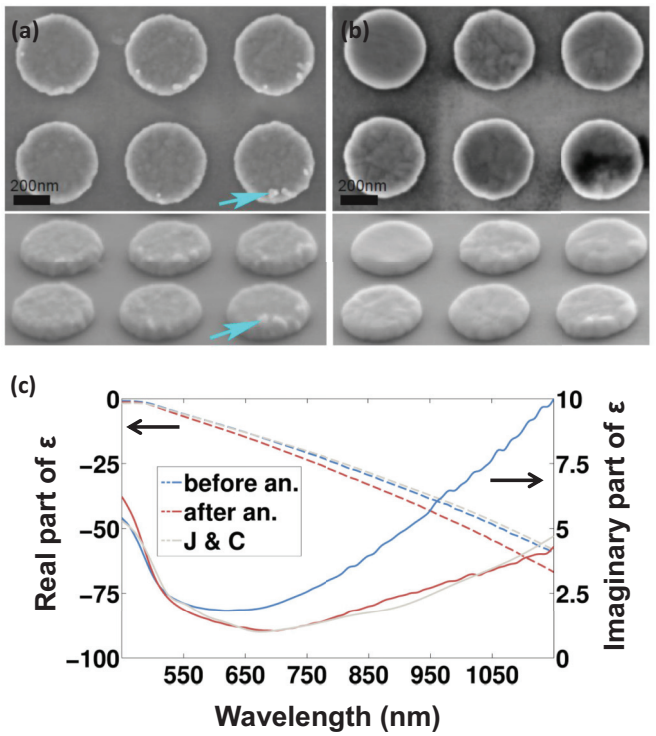

FIG. 1. (Color online) Scanning electron micrographs of gold nanodiscs (a) after liftoff and (b) after an additional annealing (200 °C for 5 min). The top panels show the top view, and the bottom panels show a view that is tilted by approximately 70°. (c) Measured values for the real and imaginary parts of the dielectric function for a thin gold film, before (blue lines) and after (red lines) the annealing process. For comparison, we also show the tabulated data of Johnson and Christy [9] (gray lines).

fitting the experimental ellipsometric data by a Bruggeman effective medium layer [10,11] with spherical inclusions, 50% volume fraction of gold, and a depolarization factor set to 1/3. Best fits are obtained for a Bruggeman layer of zero thickness. If the Bruggeman layer is set to the experimentally determined values, the resulting dielectric functions have a larger imaginary part and a smaller real part (deviations up to ∼10%) compared to those obtained with the assumption of smooth interfaces. However, the same trend upon annealing, i.e., a reduction in the real and imaginary parts, is observed.

To approach the influence of surface roughness from the experimental side, we measured the gold dielectric function on template stripped gold films [12], thus making the much smoother (rms of 0.3 nm for both annealed and unannealed films) original gold-substrate interface accessible to ellipsometric measurements (results are not shown). For these interfaces we obtain, in comparison to the original gold-air interface for annealed and unannealed films, slightly lower real parts but imaginary parts which are, within the experimental uncertainties, identical to those measured on the original gold-air interface. As for the measurements at the gold-air interface, a reduction of the dielectric function in the real and imaginary parts is also observed here upon annealing.

We find that the measured values for the dielectric function vary between samples and with time. The magnitude of these variations is on the order of the annealing-induced changes. The observed trend upon annealing, i.e., a lowering of the real and imaginary parts of the permittivity, is consistently observed in all cases investigated. The data presented in Fig. 1(c) show an example of rather large annealing-induced changes in the dielectric function and are chosen to obtain an upper estimate for their effect on the optical properties of the particles investigated below.

In the following we focus our investigations on gold nanorods, which play an important role as SERS substrates and in sensing applications [13] due to their spectral tunability and high field enhancements. The nanorods were fabricated by standard electron beam lithography [14] on a quartz glass substrate. A quartz glass substrate was chosen here as it presents a stable and well-defined dielectric environment. For conductivity during *e*-beam exposure, the layer of a positive electron resist was covered with ∼10 nm of aluminum, which was removed by a KOH solution prior to chemical resist development. After thermal vacuum deposition of gold and a liftoff process, the particles with the exposed shape remain on the substrate. Figure 2(b) depicts AFM images of two gold nanorods with approximate dimensions of 160 × 80 × 50 nm before (top panels) and after annealing (bottom panels). In contrast to SEM imaging, which has a lateral resolution on the nanometer scale, the AFM measurements are a convolution

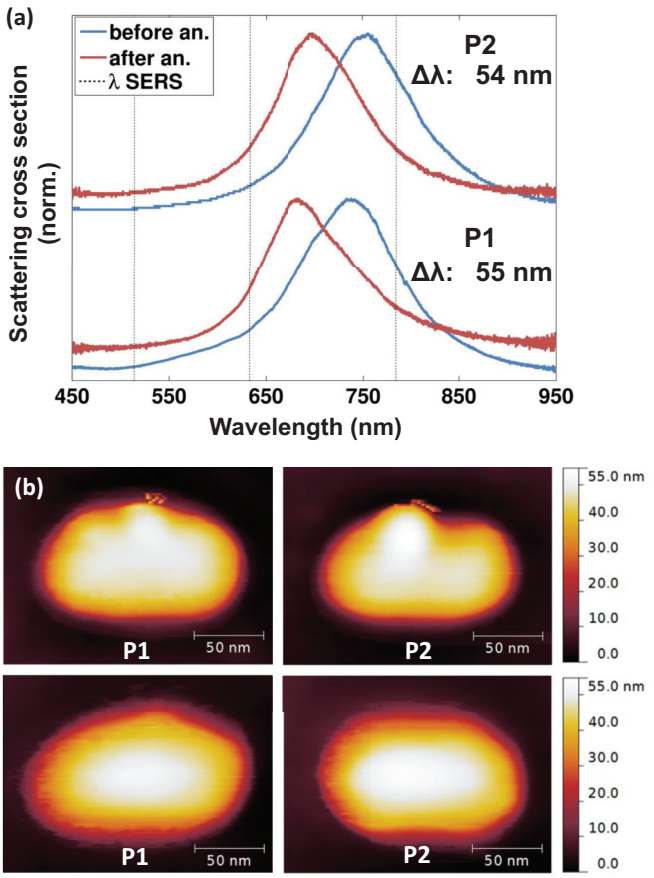

FIG. 2. (Color online) (a) Measured scattering spectra before and after annealing for two gold nanoparticles labeled as P1 and P2. The dotted lines mark the wavelengths where the SERS signal is calculated: 514, 633, and 785 nm. (b) AFM images of particles P1 and P2 before (top panels) and after (bottom panels) annealing.

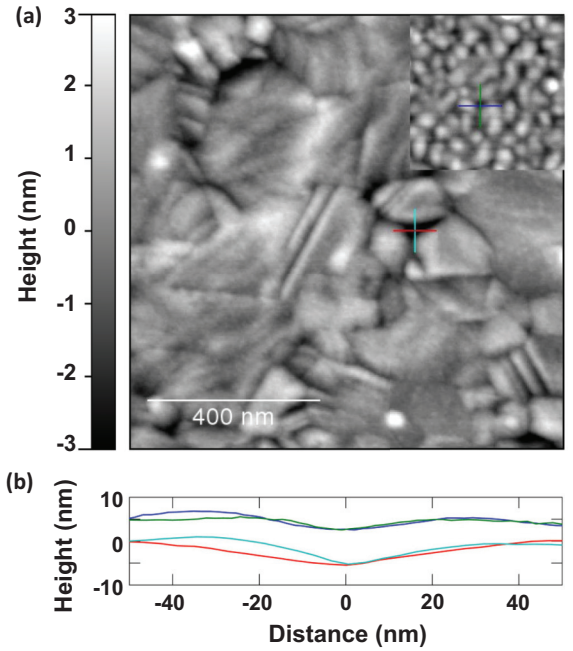

FIG. 3. (Color online) (a) Atomic force micrographs of an annealed gold-film surface (thickness of 30 nm). The inset reports the surface before annealing (same length and height scale). (b) Height profiles along the cross sections indicated in (a). The blue and green curves are vertically offset for clarity.

of the particle shapes with the AFM tip size (tip radius on the order of 10 nm). However, AFM allows us to measure a quantitative height profile of the particles, which can be used to build a geometric model of the particles (see below). For both particles, edge- and surface-roughness features can be identified.

Due to the finite tip size, deep and narrow grooves in the particle surfaces could be present without being noticed in the AFM images of the nanorods. To clarify this geometry detail, we conducted high-resolution AFM on continuous gold films with supersharp silicon tips (Team Nanotech SS-ISC, with tip radius <5 nm and a cone angle below 5°). Exemplary images are presented in Fig. 3(a). Even at the deepest observed grooves, the crosscuts through the height profile in Fig. 3(b) reveal that the surface grains touch with relatively large contact angles on the order of 170° before and after annealing [4]. This is also plausible, as the surface energy of gold-gold interfaces can be expected to be much lower than that of gold-vacuum interfaces. The difference in surface topography before and after annealing is the lateral distance between height maxima ("bump"), whose mean value is on the order of ∼20 nm before annealing and which has a very broad size distribution ranging from 20 to several 100 nm after annealing. The roughness rms value, determined over image areas of 500 × 500 nm^2, is 1.4 nm before and 0.9 nm after annealing. For a later comparison to our modeling results, we also recorded the single-particle scattering spectra of the two presented nanorods shown in Fig. 2(a) before and after annealing using a dark-field microscope with the polarization parallel to the long nanorod axes.

In summary for the experimental characterization, the particles differ geometrically from the idealized shapes through (a) surface roughness, (b) edge roughness, and (c) edge rounding. These shape parameters as well as the gold dielectric function change upon thermal annealing.

III. SIMULATIONS

Since it is not possible to separately investigate the quantitative contributions of geometric imperfections and dielectric function in experiments, a sound simulation of the investigated nanoparticles is needed. In this work we numerically solve the full Maxwell equations using the MNPBEM toolbox [15], which is based on a boundary element method (BEM) approach [16,17].

We start our analysis by comparing the annealed and unannealed gold nanoparticles shown in Fig. 2. As a first step, we generate discretized particle boundaries whose shapes are similar to the experimental ones. We extract the particle contours from AFM measurements for both cases, before and after annealing, and extrude them using the measured height profiles. For the side walls and edge rounding we use approximated values that correlate to typical edge profile shapes obtained from SEM measurements. We assume a homogeneous dielectric environment of the nanoparticle with an effective refractive index of $n = 1.23$ (weighted average between the quartz substrate and air) [5]. The dielectric functions of the gold particles are taken from our own ellipsometry measurements.

In our simulations we assume a plane-wave excitation of the nanoparticles (polarization in the direction of the long axis of the rod) and calculate the resulting scattering spectra and electromagnetic fields at the surface of the particle [15]. The convergence of the simulation results was checked by refining the surface mesh, especially around the bumps, edges, and other points of interest. For the optical spectra a total number of approximately 2500 surface elements was sufficient, whereas for the absolute values of the electromagnetic fields a much higher number of surface elements was needed (≈15 000).

In the following we report the field enhancements $|\boldsymbol{E}|$ for a plane-wave excitation with unit field strength. We additionally use $|\boldsymbol{E}|^4$ as a measure for the SERS enhancement [6] and determine both the maximum of $|\boldsymbol{E}|^4$ and the averaged $\langle|\boldsymbol{E}|^4\rangle$ value. For the averaged value we multiply $|\boldsymbol{E}|^4$ at each surface element by the corresponding element area and divide the sum by the total particle surface. Comparing the computed SERS enhancement with experiment is currently not possible because of too low signals for single lithographic nanoparticles. In the following we thus refer in the discussion to our recently published SERS study on large-particle ensembles [4].

A. Comparison with experiment

In Fig. 4 we show simulated scattering spectra for particles P1 and P2, using the measured particle shapes and dielectric functions shown in Fig. 1(c) before and after annealing. We observe two main effects upon annealing, namely, a shift of the spectral resonance position and changes of the SERS enhancement. Let us first focus on the scattering cross sections reported in Figs. 2(a) and 4(a), which show a blueshift of the resonance after annealing. Part of this shift can be attributed to the change in the dielectric function (see discussion below),

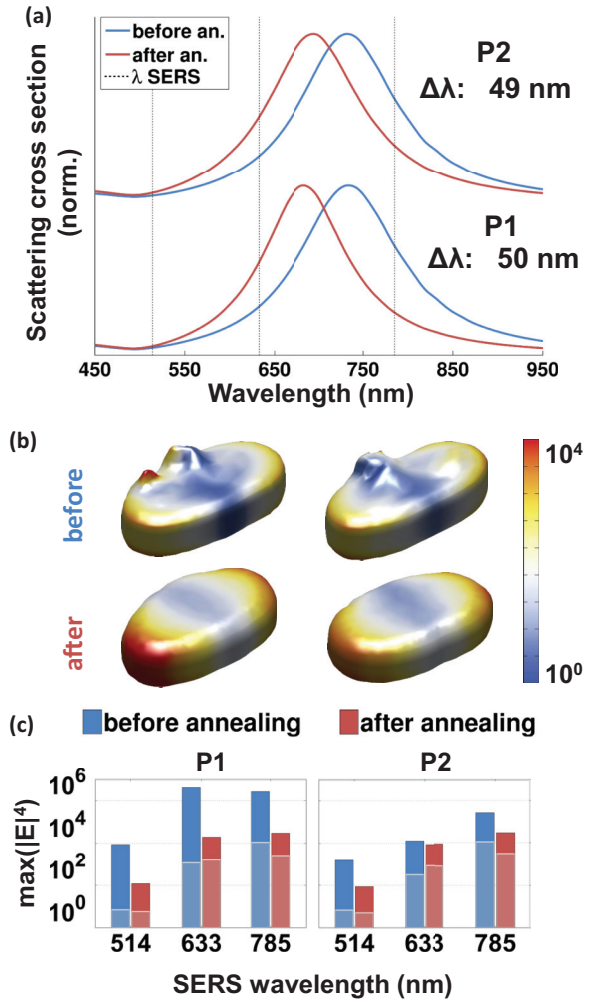

FIG. 4. (Color online) (a) Simulated scattering spectra of the gold nanoparticles P1 and P2 before and after the annealing process ($\lambda_{SERS} = 514$, 633, and 785 nm). (b) Logarithmic SERS enhancement at 633 nm before and after annealing. (c) Maximum of logarithmic SERS enhancement for both particles at different light wavelengths. The brighter parts of the vertical bars (separated by white lines) report the values averaged over the whole particle surface.

but another contribution is due to changes of the particle shape. The experimental measured peak shifts (see Fig. 2) are well reproduced in the simulation. A small remaining deviation of less than 10% can be attributed to our uncertainty in determining the exact particle shapes. Especially for nanorods, the resonance position is known to depend very sensitively on the precise aspect ratio of the particle axes [18]. Other possible reasons are the dielectric function, which is not precisely known before and after annealing, and dephasing contributions due to surface roughness scatterings [19] missing in our simulation approach.

In Fig. 4(c) the calculated maxima and mean SERS enhancements of the two investigated particle geometries are plotted. We use representative SERS wavelengths of 514, 633, and 785 nm. For the maximum SERS, we get a decrease after annealing of one to two orders of magnitude, a finding that agrees at least qualitatively with the experimental observations [4]. Note that the values from the simulations are of the same order of magnitude as estimated SERS enhancement factors for larger arrays of gold nanoparticles [20].

To disentangle the contributions of the different effects, in the following we analyze them separately by subsequently altering the dielectric function and geometric details of the gold nanorod while keeping the nanorod cross section (45 nm in width and 25 nm in height) as well as the edge rounding of 5 nm constant.

B. Change in dielectric function and resonance position

Heating a nanoparticle or metallic film leads to thermal curing, where bumps and surface imperfections diminish, but it also inevitably modifies the grain sizes of the metal and, in turn, the dielectric properties [4,7]. The annealing-induced changes of the dielectric function reported in Fig. 1(c) depend on the wavelength. To assess the corresponding changes of the particle plasmon resonance, we analyze different resonance positions by varying the length of a smooth nanorod from 80 to 120 nm. In Fig. 5(a) the effects of this dielectric change on the scattering cross section are plotted. There is a clear trend for the plasmon resonance; namely, the peaks blueshift by about 20 nm, and the peak heights increase because of the decrease of the imaginary part of the modified dielectric function.

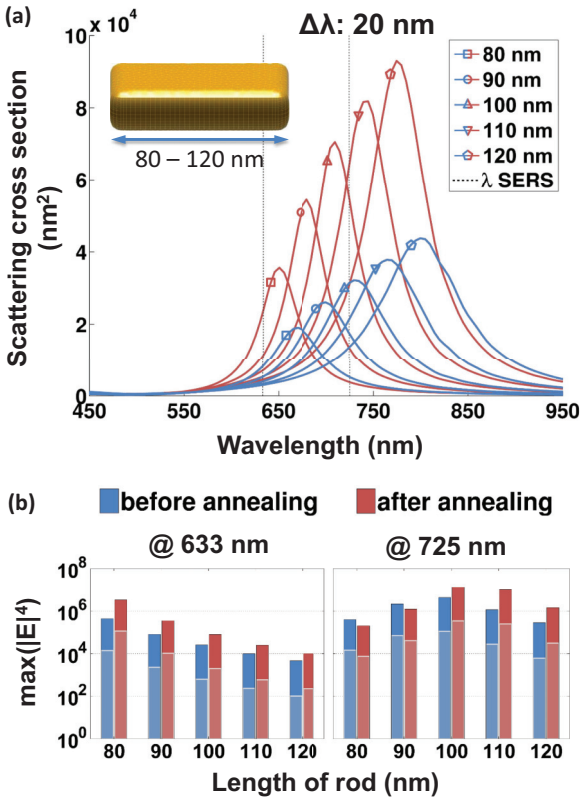

FIG. 5. (Color online) (a) Scattering cross sections of gold nanorods with different particle lengths (width of 45 nm, height of 25 nm) and using the dielectric function from Fig. 1(c). The blue and red lines show results for the particles before and after annealing, respectively. (b) Maximum of logarithmic SERS enhancement for the same rods evaluated at two different wavelengths indicated in (a). The brighter parts of the vertical bars (separated by white lines) report the averaged SERS enhancements.

The modified dielectric function also influences the SERS enhancements, as shown in Fig. 5(b), where we compute the SERS maxima for all five rod lengths at two different wavelengths. Quite generally, we get the highest SERS enhancement for the structures whose plasmon resonance is closest to the considered SERS wavelength. Let us elucidate this with the example of the highest values in the right panel of Fig. 5(b), i.e., rod lengths of 100 and 110 nm. A comparison with the scattering spectra in Fig. 5(a) reveals that the corresponding resonance wavelengths λ_{SSP} are closest to the considered SERS wavelength of $\lambda_{SERS} = 725$ nm (dotted lines). For these rod lengths the SERS enhancement decreases upon annealing because the plasmon resonance shifts away from λ_{SERS}. The trend is reversed for the shorter rod lengths of 80 and 90 nm, where λ_{SSP} moves closer to λ_{SERS}. For the SERS wavelength $\lambda_{SERS} = 633$ nm [left panel of Fig. 5(b)], we find that annealing always leads to an increase of the SERS enhancement because the resonance wavelengths λ_{SSP} of all nanorods move closer to λ_{SERS}.

C. Surface roughness

In Ref. [5] we showed that the surface plasmon averages over the random height fluctuations of a rough metallic particle, which leads to destructive interference and an overall small net effect in the optical far field. However, the near-field enhancement can critically depend on the details of the roughness features. As discussed in the experimental section, typical roughness features on the particles' top surface are often rather smooth, with grain dimensions of ∼20 nm lateral size and height fluctuations between 1 and 2 nm. From experiment we do not observe any larger protrusions (Fig. 3), which might give rise to considerable geometric enhancement.

To simulate typical surface-roughness effects in the near field, in the following we focus on one single notch shown in Fig. 6 to account for the boundary of surface grains (compare to crosscuts shown in Fig. 3). In agreement with Ref. [5] we find that the notch has no significant influence on the scattering spectra. Also the influence on $\langle |\boldsymbol{E}|^4 \rangle$ is surprisingly small. Only when the notch is placed at the edge corner of the particle, an increase of the $|\boldsymbol{E}|^4$ maximum by approximately 50% is observed.

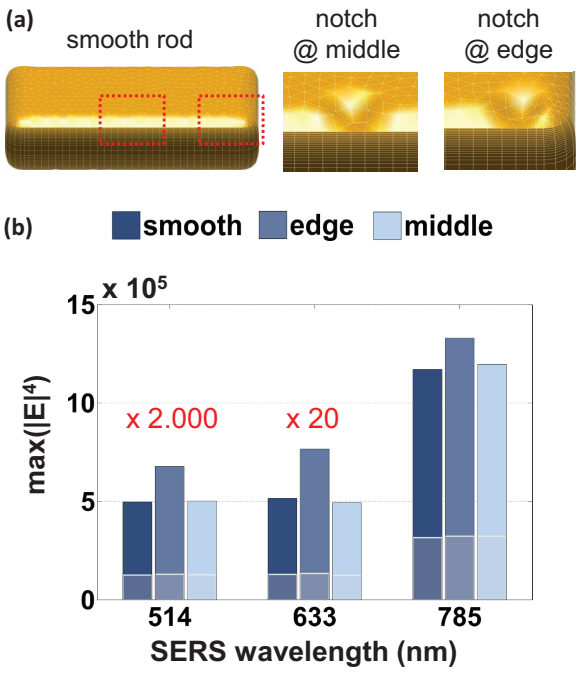

FIG. 6. (Color online) (a) Smooth surface of a gold nanorod with dimensions of $100 \times 45 \times 25$ nm^3. The particle is modified by a small notch placed at the corner and in the middle of the structure, respectively, to investigate the influence of surface imperfections (see magnified images of the dotted regions on the right). The scattering spectra (not shown) are almost identical for all three particle shapes. (b) Maximum of $|\boldsymbol{E}|^4$ for the smooth surface and the two particles with the notch placed at the edge and in the middle for three SERS wavelengths. The brighter parts of the bars indicate the averaged SERS enhancement. Multiplication factors of 20 and 2000 have been used for the shorter wavelengths.

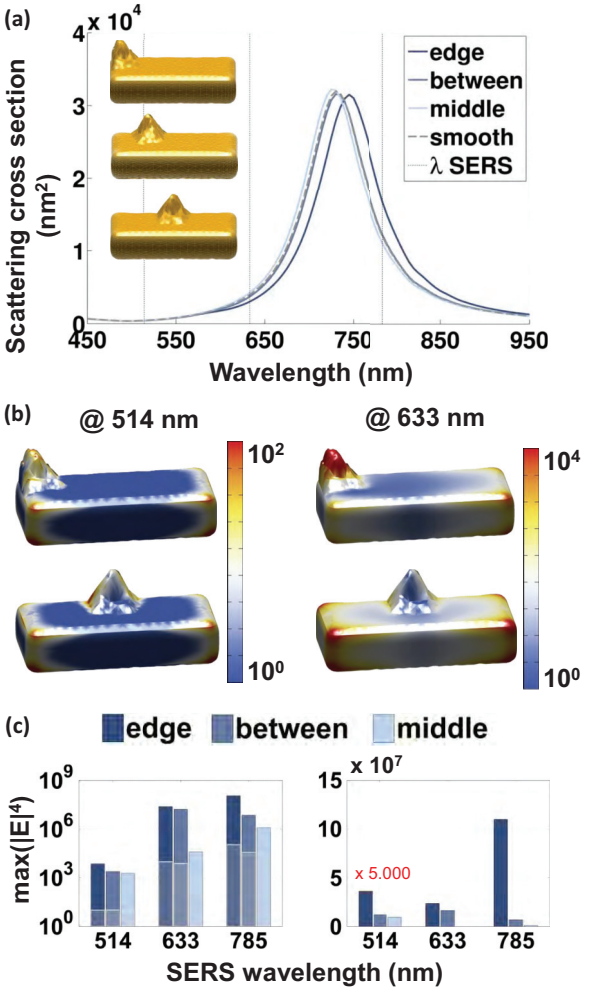

FIG. 7. (Color online) (a) Scattering spectra of a gold nanorod ($45 \times 25 \times 100$ nm^3) with bumps at three different positions. The spectrum of the smooth particle is given by the dotted line. (b) Logarithmic SERS enhancement for two bump positions at two different wavelengths. (c) Maximum SERS enhancement for all three bump positions at different wavelengths (logarithmic scale on the left-hand side). The bars at 514 nm in the bottom right panel have been multiplied by a factor of 5000 to make them visible.

D. Edge roughness

We finally discuss the edge-roughness features identified experimentally. The above results for the notch already indicated that the near field becomes enhanced primarily at positions where the plasmon mode density is high. To further corroborate this point, we investigate in Fig. 7 a nanorod with a pronounced roughness feature, here a bump similar to the experimentally observed ones, at three different positions. For the optical spectra the bump has no significant impact on the resonance wavelength, with the exception of a small shift for the edge bump. The SERS enhancement, on the other hand, increases the closer the bump moves to the nanorod ends with a high plasmon mode density. At a wavelength of 785 nm the maximum of $|\boldsymbol{E}|^4$ is two orders of magnitude higher than for the other bump positions.

IV. DISCUSSION

The results presented above identify various contributions to the optical far-field response and SERS enhancement of gold nanorods. A major contribution to the optical near-field and SERS enhancement results from typical edge-roughness features (local protrusion of ∼20 nm extension), provided that they are situated at regions of large plasmonic mode density. Although they only occupy a small surface region of the nanoparticle, the contribution can dominate even the average SERS signal. In contrast, surface roughness on the top side of the particle gives only small contributions to the $|E|^4$ enhancement, say of the order of ±50% compared to typical values of an ideally smooth particle, and has almost no impact on the averaged SERS enhancement. On the other hand, all these geometric imperfections have only a minor influence on the far-field scattering spectra.

In contrast, the dielectric function and its change upon annealing clearly affect the scattering spectra. In particular the reduced imaginary part leads to a strengthening of the resonance, whereas the reduced real part leads to a blueshift of the resonance. Both changes also influence the optical near-field and SERS enhancement. The latter scales roughly with the square of the scattering cross section and, for resonant excitation, can lead to an average SERS enhancement of about a factor of 4 compared to the unannealed particle.

It should be noted that the presented calculations are only semiquantitative because the modeled structures are not identical to the real ones. The assumption of an effective and homogeneous surrounding instead of the real plane substrate as well as inevitable discrepancies between the real and modeled particles can cause deviations with respect to the experimental results. Nevertheless, our results highlight that the SERS signal of an array of lithographic particles critically depends on the exact location and total number of roughness features, as well as the particles' dielectric function. Annealing reduces edge roughness and the accompanying SERS enhancement but also enhances the SERS signals due to lower Ohmic damping of the plasmon resonance. Depending on the relative importance of these various effects on an actual sample under investigation, annealing can either lead to a reduction of the average SERS signal (as usually observed experimentally) or lead to an enhancement (to be expected in the red spectral range, on lithographic arrays with little or no edge-roughness features).

ACKNOWLEDGMENT

This work has been supported in part by the Austrian science fund (FWF) under Projects No. P24511, No. P21235–N20, and No. P25034–N20, and the SFB NextLite.

[1] J. Rodriguez-Fernandez, A. M. Funston, J. Perez-Juste, R. A. Alvarez-Puebla, L. M. Liz-Marzan, and P. Mulvaney, Phys. Chem. Chem. Phys. **11**, 5909 (2009).
[2] K.-P. Chen, V. P. Drachev, J. D. Borneman, A. V. Kildishev, and V. M. Shalaev, Nano Lett. **10**, 916 (2010).
[3] W. L. Barnes, J. Opt. A **11**, 114002 (2009).
[4] J.-C. Tinguely, I. Sow, C. Leiner, J. Grand, A. Hohenau, N. Felidj, J. Aubard, and J. R. Krenn, BioNanoScience **1**, 128 (2011).
[5] A. Trügler, J.-C. Tinguely, J. R. Krenn, A. Hohenau, and U. Hohenester, Phys. Rev. B **83**, 081412(R) (2011).
[6] E. C. Le Ru, J. Grand, N. Felidj, J. Aubard, G. Levi, A. Hohenau, J. R. Krenn, E. Blackie, and P. G. Etchegion, J. Phys. Chem. C **112**, 8117 (2008).
[7] M. J. Rost, D. A. Quist, and J. W. M. Frenken, Phys. Rev. Lett. **91**, 026101 (2003).
[8] D. W. Lynch and W. R. Hunter, in *Handbook of Optical Constants of Solids*, edited by E. D. Palik, Vol. II (Academic Press, New York, 1985), p. 286.
[9] P. B. Johnson and R. W. Christy, Phys. Rev. B **6**, 4370 (1972).
[10] G. A. Niklasson, C. G. Granqvist, and O. Hunderi, Appl. Opt. **20**, 26 (1981).
[11] G. A. Niklasson, Sol. Energy Mater. **17**, 217 (1988).
[12] N. Vogel, J. Zieleniecki, and I. Köper, Nanoscale **4**, 3820 (2012).
[13] A. Jakab, Y. Khalavka, J. Becker, A. Trügler, C. Rosman, U. Hohenester, and C. Sönnichsen, ACS Nano **5**, 6880 (2011).
[14] M. McCord and M. Rooks, *Handbook of Microlithography, Micromachining and Microfabrication*, Vol. 1 (SPIE, Bellingham, WA, 1997).
[15] U. Hohenester and A. Trügler, Comput. Phys. Commun. **183**, 370 (2012).
[16] F. J. Garcia de Abajo and A. Howie, Phys. Rev. B **65**, 115418 (2002).
[17] U. Hohenester and J. R. Krenn, Phys. Rev. B **72**, 195429 (2005).
[18] J. Becker, A. Trügler, A. Jakab, U. Hohenester, and C. Sönnichsen, Plasmonics **5**, 161 (2010).
[19] U. Kreibig and M. Vollmer, *Optical Properties of Metal Clusters*, Springer Series in Materials Science Vol. 25 (Springer, Berlin, 1995).
[20] G. Laurent, N. Felidj, J. Aubard, G. Lévi, J. R. Krenn, A. Hohenau, G. Schider, A. Leitner, and F. R. Aussenegg, Phys. Rev. B **71**, 045430 (2005).